Atomic structure of the interface between silicon (111) and amorphous germanium

N. I. Borgardt,* B. Plikat,† W. Schröter, and M. Seibt‡
IV. Physikalisches Institut der Universität Göttingen and Sonderforschungsbereich 602, Friedrich-Hund-Platz 1, D-37077 Göttingen, Germany

Th. Wagner
Max-Planck-Institut für Metallforschung, Heisenbergstr.3, D-70569 Stuttgart, Germany
(Received 28 May 2004; published 8 November 2004)

The structure of the transition region between crystalline Si(111) and amorphous germanium has been studied by means of quantitative high-resolution electron microscopy. Using iterative image matching techniques the two-dimensional distribution function of germanium atoms in the transition region has been determined from focal image series of such interfaces. The distribution function reveals lateral ordering close to the crystalline substrate in addition to a pronounced layering usually observed for solid-liquid interfaces. It further shows that the transition region is elastically strained due to the volume misfit between crystalline silicon and amorphous germanium. The width of the transition region is 1.4 nm corresponding to about four (111) layers of crystalline silicon or germanium. Finally, the width of the bond-angle distribution for the first layer of germanium atoms on the silicon substrate is determined as 8.9° which is close to the corresponding value of 9.7° for bulk amorphous germanium.

DOI: 10.1103/PhysRevB.70.195307 PACS number(s): 68.35.Ct, 68.35.−p, 68.37.Lp

I. INTRODUCTION

It is a long-standing problem to measure the structure of interfaces between crystalline and amorphous materials (c/a interface). Such interfaces play an important role for various physical processes, e.g., crystallization of amorphous materials or amorphization of crystalline solids by ion implantation,[1] solidification of rapidly cooled melts after laser irradiation,[2] and low-temperature molecular-beam epitaxy of semiconductors.[3] In addition, crystalline-amorphous interfaces are important for various devices such as, e.g., metal-oxide semiconductor field-effect transistors (MOSFET's) (Ref. 4) or spin-dependent tunneling junctions.[5] There interfaces between crystalline semiconductors or metals and amorphous oxides are an integral part of the device. Their behavior is increasingly governed by the properties of the interfaces especially when the layer thickness approaches the subnanometer regime.[4,6]

Crystalline-amorphous interfaces structurally mediate between materials with qualitatively different atomic ordering, i.e., long-range order on the crystalline and a complex structure described in terms of atomic correlations on different length scales as *short-range* and *medium-range order*.[7] Experimentally, short-range order is well accessed by diffraction techniques which allow us to measure the *radial distribution function* (RDF), closely related to the pair-correlation function, whereas information on medium-range order can be obtained from extended x-ray-absorption fine structure[8] or variable coherence microscopy.[9,10]

In regions close to crystalline substrates long-range correlations of atom positions will occur in the disordered material due to the underlying translational symmetry. In this so-called *transition region* perfect crystalline order will decay to the short-range and medium-range order of the bulk amorphous material. Due to the lack of radial symmetry in the transition region, the RDF is of limited use when the atomic structure is to be described. Following a procedure usually applied to describe the time-averaged structure of solid-liquid interfaces[11] a three-dimensional atomic densitiy $\rho_{3D}(x,y,z)$ can be formulated where x is chosen as the direction perpendicular to the interface and the yz plane is parallel to the interface. For solid-liquid interfaces theoretical investigations and computer simulations (see Ref. 12 for a review) as well as experimental observations[13] show that atomic density profiles $\rho_x(x)$ averaged along the interface indicate a pronounced layering of the liquid close to the substrate. In addition, recent molecular-dynamic simulations[14] demonstrate the existence of a crystal-like order in the yz plane of liquid layers.

Various theoretical techniques have been applied to the study structure and properties of interfaces and transition regions in covalently bonded systems[15–21] as well as interface mediated crystallization and amorphization[22,23] or oxidation processes[24] of silicon. Simple interface properties extracted from such calculations, however, are considerably different depending on the theoretical technique as well as on the preparation of the c/a interface. As an example, let us consider the width of the transition region between crystalline silicon and bulk amorphous silicon. By calculating the excess energy density Tu *et al.*[17] come up with a decay length of the crystalline order of 0.3 nm [one (111) double layer] for the Si(111)/a-Si interface. By means of tight-binding simulations Bernstein *et al.*[16] estimate 0.7 nm for the Si(001)/a-Si interface using the bond-angle distribution as a criterion whereas da Silva *et al.*[21] extract a value of 1.1 nm from Monte Carlo simulations of the same interface.

Crystalline-amorphous interfaces are difficult to access experimentally since high-resolution scanning probe microscopies are not suitable for buried interfaces leaving high-resolution electron microscopy (HREM) as the method of choice. It has primarily been applied to the interface between

crystalline silicon and amorphous SiO_2 in order to study its roughness[25] and structure,[26–29] which is of outstanding importance for conventional silicon microelectronics. Ohdomari *et al.*[26] recognized, by using conventional image simulations based on atom positions extracted from a hand-built ball-and-sticks model of a continuous random network (CRN) of a-SiO_2 attached to (111)Si, that the position of the c/a interface as determined from intuitive interpretation of HREM images is shifted to the amorphous side relative to the true interface position. From a comparison of simulated and experimental images taken in cross section Ourmazd *et al.*[27] conclude that a strained, trydimitelike SiO_2 is formed directly on top of silicon which then gradually transforms into the amorphous bulk phase within three atomic layers. This interpretation has been questioned by Akatsu *et al.*[28] who interpret similar image contrasts in terms of a faceted $Si(001)/a$-SiO_2 interface. Recently, again using HREM, Ikarashi *et al.*[29] conclude the existence of a crystalline SiO_2 layer which is proposed to have a crystoballitelike structure.

Besides the c-Si/a-SiO_2 interface, HREM was applied to examine the interface between crystalline Pd_3Si and amorphous $Pd_{80}Si_{20}$.[30] Based on the qualitative comparison of the contrast in experimental and simulated images and intensity profiles for a single defocus value it was concluded that atomic ordering extends in the first several layers of the amorphous material adjacent to the crystalline material.

Common to all of these studies is the direct qualitative comparison of experimental images with simulations which are calculated for a specific arrangement of atoms in the amorphous part of the interface[26,30] or ignoring the atomic arrangement at all.[27–29]

We have developed a method which allows us to determine the two-dimensional projection $\rho(x,y)$ of $\rho_{3D}(x,y,z)$ along the electron beam from HREM micrographs of crystalline-amorphous interfaces taken in cross-section geometry.[31] The approach consists of the evaluation of averaged interface images obtained by averaging intensities at distances of the crystal periodicity along the interface direction. Experimental defocus series of averaged images are compared to simulated images which are calculated using the *multislice* algorithm[32] within the *averaged projected potential* (APP) approximation.[31] The latter uses the two-dimensional distribution function $\rho(x,y)$ describing the projected density of atoms in the amorphous material to directly calculate averaged images which drastically reduces the computational load of image simulation. As a result, iterative image matching techniques[33,34] can be applied for structure determination. In order to reliably separate effects arising from Fresnel diffraction ("delocalization") from structural features the iterative image matching is extended to whole focal image series consisting of 20 images. Such series have previously been used to retrieve amplitude and phase of the electron wave.[35]

In our preliminary analysis of HREM images obtained from the c-$Si(111)/a$-Ge interface the distribution function $\rho(x,y)$ in the transition layer either was assumed to be homogeneous or was calculated based on the radial distribution function of the bulk amorphous material.[31] A comparison of the calculation results with the experiment clearly showed that such approaches are insufficient and it also showed that the short-range order in the amorphous layer in the vicinity of the boundary with the crystal and far from it are substantially different from each other.

In this work we present the first quantitative determination of the two-dimensional distribution function $\rho(x,y)$ of the transition region of amorphous germanium grown by low-temperature molecular beam epitaxy on unreconstructed Si(111) substrates. We show that the width of the transition region is 1.4 nm corresponding to about four (111) layers of crystalline silicon or germanium. The atomic distribution function shows maxima at positions that correspond to atom positions in a crystalline germanium thin film pseudomorphically grown on Si(111). Hence it can be concluded that the transition region is elastically strained due to the misfit between crystalline silicon and amorphous germanium. Finally, the width of the bond-angle distribution for the first layer of germanium atoms on the silicon substrate is determined as 8.9°. This value is close to the corresponding value of 9.7° for bulk amorphous germanium.

In Sec. II we describe experimental details as well as the method used to extract statistical information from experimental images. Subsequently, the procedure of iterative image matching and its results are presented in Sec. III. In order to construct the distribution function $\rho(x,y)$ in terms of a small number of parameters, we use a recursive scheme treating the transition region as consisting of layers starting at the last crystalline lattice plane (Sec. III A). Section III B provides details of the iterative image matching procedure used in this work. It extends previous applications in the sense that a whole series of HREM images are matched simultaneously. The results of iterative image matching are described and discussed in Sec. III C.

II. EXPERIMENTAL IMAGES OF THE INTERFACE AND THEIR AVERAGING

For the investigation of the short-range order near c/a interfaces we prepare an atomically flat $Si(111)/a$-Ge interface. Germanium was evaporated on a $Si(\bar{1}11)$ surface with a misorientation of less than 0.1° in the $[11\bar{2}]$ direction as determined with atomic force microscopy by Suhren *et al.*[36] who kindly provided pieces of their starting material. Following their experimental procedure after removal of 100-nm thermal oxide we smoothed the Si(111) surface by etching in 40% NH_4F and finally rinsed in DI water. This results in hydrophobic unreconstructed terraces.[36,37] The investigated interface was produced by room-temperature deposition of germanium from an electron gun heated crucible. The growth rate was 3 nm per minute.

Cross-section specimens along $Si[1\bar{1}0]$ were prepared by mechanical thinning followed by ion-beam thinning with 3-keV Ar ions at 10° incidence angle. The TEM work was done using a Philips CM200 UT-FEG with an acceleration voltage of 200 kV. The microscope has a point resolution of 0.19 nm and an information limit of 0.11 nm. Images were

taken using an objective aperture with a diameter corresponding to 24 mrad including {111} and {200} reflections of the silicon substrate. Through-focus series with 20 images were recorded using a GATAN SSC charge-coupled device (CCD) (Model 694) and specimen drift was corrected using cross correlations of successive images in the series.

In order to obtain structural information on the atomic scale experimental HREM images have to be compared to the simulated ones. Such a comparison is a routine procedure in the investigation of crystalline materials. Here, image simulations not only allow us to explain the image contrast but also to retrieve quantitative structural and chemical data from HREM images. However, a direct application of the procedure to the investigation of crystalline-amorphous interfaces is not possible since the position of atoms in amorphous materials are known only with a certain probability. Even when the probabilities of the atom distributions are known, simulated and experimental images cannot directly be compared with each other since the amorphous layer with the definite short-range order will have a great variety of specific realizations.

An appropriate way to extract structural information is to compare HREM images of c/a interfaces which have been spatially averaged along the boundary.[31] Such averaged images are sensitive to the mean distribution of the projected potentials of atoms in the amorphous layer close to the crystalline substrate.

HREM images of c/a interfaces can be averaged by two methods. In the first method the averaged images of the interface are calculated [Figs. 1(a) and 1(b)]. The interface image [Fig. 1(a)] is divided into N stripes perpendicular to the interface with width d which is the period of the lattice image parallel to the interface. This direction will subsequently referred to as the y axis. Averaging over equivalent points of these stripes gives the intensity distribution in the averaged interface image,

$$I'(x,y) = \frac{s_d(y)}{N} \sum_{n=-(N-1)/2}^{(N-1)/2} I(x,y+nd), \tag{1}$$

where $I(x,y)$ is the intensity distribution in the original HREM image and $s_d(y)$ is the slit function equal to 1 for $-d/2 \leqslant y < d/2$ and zero elsewhere. The averaged interface image is shown in Fig. 1(b).

In studying the near interfacial order in amorphous materials it is important to choose the width of the averaging strip to be equal to the period of the mean distribution of the atom potential projected along the electron beam. Since the distribution periodicity along the interface is caused by the crystal translation symmetry it can be expected that the periods of the projected potential distribution in the crystalline and amorphous parts coincide with each other. Such a guess is confirmed by direct Fourier analysis of the intensity variations along the y axis in the crystalline and amorphous regions of the interface image in the vicinity of the boundary. Figures 1(c) and 1(d) show Fourier transforms $|F\{I_1(y)\}|$ and $|F\{I_2(y)\}|$ which were calculated for the intensity distributions $I_1(y)$ and $I_2(y)$ along the directions denoted by arrows 1 and 2 in Fig. 1(a), respectively. For convenience, the dependencies are normalized with respect to values $|F\{I_1(y)\}|$ and $|F\{I_2(y)\}|$ at $k_y=0$. In the figure it can be seen that the Fourier transform differs essentially from zero near the spatial frequencies close to $\pm 1/d$. That means that the period of the intensity variations along the interface in the crystalline and near-to-the boundary amorphous regions coincide and are equal to d. It should be noted that for $|F\{I_1(y)\}|$ unlike $|F\{I_2(y)\}|$ has a contribution at frequencies close to $\pm 2/d$. Absence of higher frequency contributions to the Fourier transform is associated with the size of the microscope objective aperture.

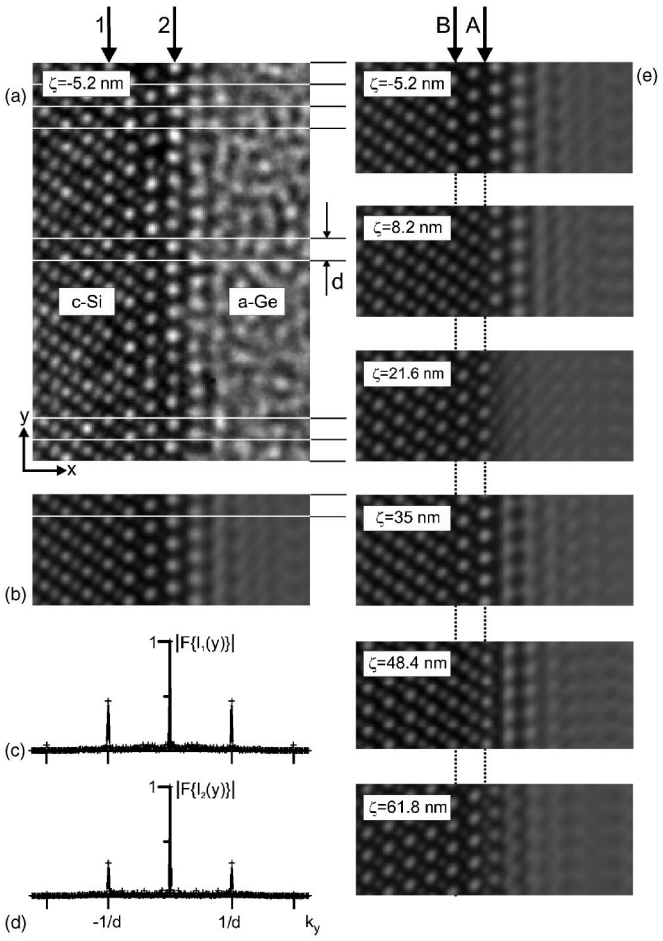

FIG. 1. Evaluation of averaged images: (a) HREM image of the c-Si(111)/a-Ge interface with illustration of its averaging with a period d, (b) resulting average image repeated five times for better visualization, (c) and (d) Fourier transforms of the intensity distributions in the HREM image along directions shown by the arrows 1 and 2 in (a), respectively, (e) some of the averaged images obtained from through-focus series of HREM images; arrow A indicates the position of the c/a interface intuitively determined from the minimum-contrast image at $\zeta=21.6$ nm whereas arrow B shows the true interface position determined from iterative image matching of the whole focus series.

In the second method of averaging the intensity profile $I(x)$ obtained from the region $A=Nd$ extended along the y axis is to be calculated as

$$\overline{I}(x) = \frac{1}{A}\int_{-A/2}^{A/2} I(x,y)dy. \quad (2)$$

The use of the intensity profiles is convenient for the visual comparison of simulation results with experiments and will be used for this purpose throughout this paper. It should be noted, however, that iterative image matching procedures used in this work, averaged *images* as calculated by Eq. (1), have been used for the quantitative comparison.

The averaged images and the intensity profiles were obtained for all 20 images of a through-focus series. The size of the averaging region was 15.6 nm and included $N=47$ stripes. Some of the averaged images are shown in Fig. 1(e). The defocus values and the specimen thickness which is equal to 13.8 nm were found by the well-known iterative procedure of simulation and numerical comparison between simulated and experimental images.[33,34]

The images were compared with each other in the crystalline part of the interface for the total through-focus series until the best set of parameters was found. From Fig. 1(e) it can be seen that the averaged intensity distributions have a regular character and in particular are free from the influence of the random overlap of projected atom potentials in the amorphous part of the interface which give rise to the speckle pattern in the original experimental images [cf. Fig. 1(a)]. Hence averaged experimental images carry statistical information and can be compared with simulated images calculated on the basis of $\rho(x,y)$.

At a defocus value of $\zeta=21.6$ nm the contrast of the amorphous region is minimal[38] [see Fig. 1(e)]. Such images are frequently used for an intuitive determination of the position of the last atomic layer belonging to the crystalline material. This position is shown by arrow A in Fig. 1(e). It will be seen below that the true position of the boundary between the crystal and the amorphous layer is significantly more to the left of arrow A and in reality the crystal boundary atoms are located along the straight line indicated by arrow B.

III. IDENTIFICATION OF THE NEAR INTERFACIAL SHORT-RANGE ORDER

A quantitative investigation of the atomistic structure of materials by means of HREM is commonly performed by iterative image matching procedures where the positions of atoms are determined by simulating the images and comparing the simulation results with the experiment (see Refs. 33 and 34 for reviews). Conventional methods of HREM image simulation need the specification of atom positions in the specimen, division of the latter into thin slices normal to the electron beam, calculation of the projected potentials of atoms for each slice, and the description of the electron scattering by the set of two-dimensional potentials in each slice. That type of simulation—which will be further referred to as *atomistic simulation*—is an established procedure for crystalline specimens. An atomistic simulation of HREM images from crystalline-amorphous interfaces, in addition, must include the determination of atom positions in the amorphous part of the interface, which can be performed with the use of, e.g., continuous random network or molecular-dynamics simulations. In order to match the size of experimentally accessible averaging regions such calculations have to be performed on systems containing 10^4-10^5 atoms which is not feasible by current computers. This is especially true if complicated interatomic potentials have to be used as in the case of covalent semiconductors. The perspective of iterative image matching significantly adds to this problem.

Simplification in simulating the averaged HREM images is attained by using the *average projected potential* approximation in multislice calculations,[31] where the two-dimensional distribution function $\rho(x,y)$ in the amorphous part of each thin slice of the specimen is used instead of the actual atomic position. Such an approach allows sufficiently accurate image simulations while reducing the computational load by approximately three orders of magnitude. It also allows us to characterize the partial order on the amorphous side of the interface in a compact form representing the distribution of interatomic bond lengths and angles.

The remaining problem to be solved is thus the calculation of the two-dimensional distribution function $\rho(x,y)$ describing the amorphous part of the interface. The application of iterative image matching procedures requires the expression of this distribution function in terms of a small number of structure-sensitive parameters which, in addition, should be extractable from structure calculations on the basis of, e.g., continuous random network or molecular-dynamics simulations.

For this purpose, a recursive scheme for determining the atomic density $\rho_{3D}(x,y)$ and further the two-dimensional distribution function $\rho(x,y)$ has been developed (Sec. III A). Our approach takes into account the translation symmetry of the crystalline substrate and the directionality of covalent bonds between atoms in the amorphous part of the interface. The calculation starts from the boundary atoms of the crystal which are assumed to be undisturbed, i.e., we effectively use a *rigid-substrate approximation* frequently applied in studies of solid-liquid interfaces. The model has two free parameters in its simplest version which is used throughout this work.

In this section (Sec. III A) we first introduce the recursive scheme for calculating the two-dimensional distribution function and explain the meaning of the free parameters which are adjusted by the structure refinement procedure described in Sec. III B. The optimum two-dimensional distribution function and the corresponding parameters of the structure model obtained by this procedure are presented in Sec. III C.

A. Models of the mean distribution of germanium atoms

The modification of the near interfacial order is caused by the translational symmetry of the crystal atoms, which, together with the directionality of covalent bonds between the germanium atoms, determines the structure of the transition region. The two factors mentioned underlie the building of the models for finding the two-dimensional distribution function in the amorphous layer. The models suggest that the mean spatial orientation of bonds between germanium atoms

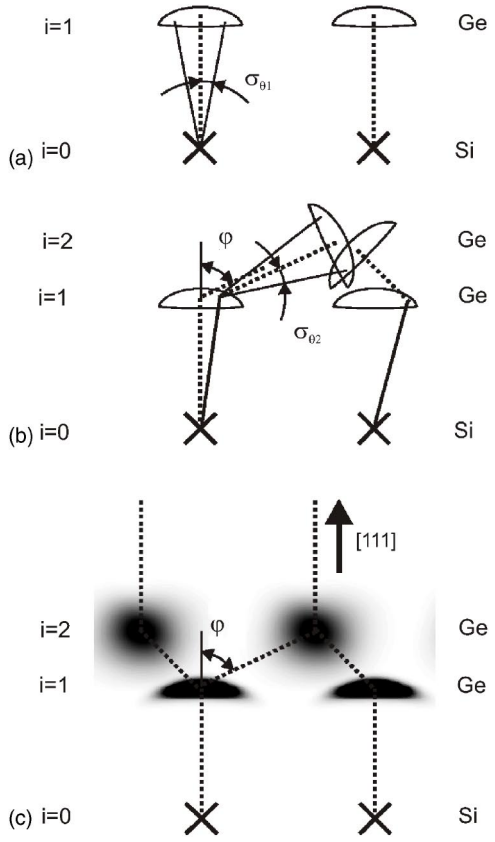

FIG. 2. Illustration of the recursive scheme used to construct the three-dimensional atomic density $\rho_{3D}(\mathbf{r})$ (a, b) and the two-dimensional distribution function $\rho(x,y)$ (c) for the first and second germanium layers. (a) Starting from the crystalline substrate denoted by layer number $i=0$ (atom positions indicated by crosses) the mean orientation of bonds to the next layer ($i=1$) is defined (vertical dotted line). The distribution of bond directions is assumed to be a Gaussian with the standard deviation $\sigma_{\theta 1}$ indicated by the cone in (a). (b) The mean orientation of bonds from layer $i=1$ to $i=2$ is inclined by an angle φ; again a Gaussian distribution (standard deviation: $\sigma_{\theta 2}$) of bond directions is assumed as indicated by the cones. The solid lines show two possible orientations of bonds between silicon and germanium atoms; note that the bonds are shown in projection along the $[1\bar{1}0]$ direction. (c) projection of the atomic density $\rho_{3D}(\mathbf{r})$ along the electron-beam direction.

can be specified relative to the bond directions in the underlying silicon substrate (see below). Bearing in mind that there is a volume misfit between crystalline silicon and amorphous germanium we distinguish two models which assume either an elastic distortion of the transiton region as a response to the misfit (model 1) or an undistorted transition region implaying relaxation of the misfit (model 2). For model 1 the mean spatial orientation of the bonds is not ideal and the angle between the [111] direction and the mean direction of covalent bonds inclined to the boundary is approximately $\varphi=65°$ instead of $\varphi=70.5°$ as is the case in the ideal diamond lattice (see Fig. 2). The corresponding mean orientation of the bonds in the transition region will be referred to as the model with tetragonal distorted bonds.

For model 2 the mean spatial orientation of covalent bonds corresponds to the ideal case, i.e., $\varphi=70.5°$. Such a model for the mean orientation of bonds will be referred to as the model with an ideal orientation of bonds.

Introducing the mean spatial orientations of bonds in the amorphous layer allows us to transform spatial orientations of bonds between atoms from the discrete set of directions in the crystal into the mean homogeneous distribution in the bulk amorphous material in a gradual manner. Both of the models assume that the boundary atoms of the silicon crystal are bonded to the atoms of the amorphous layer without inserting dangling bonds or changing the number of bonds to any atom. The bond directions of the boundary silicon atoms remain to be close to the ideal tetrahedral orientations. It should be emphasized that the models do not allow us to find a concrete realization of germanium atom positions. Instead, they allow us to obtain the mean atom distribution which permits the occurrence of the tetrahedrally bonded atom structure. This is a necessary condition for successful modeling of the atom structure of amorphous germanium.[39]

After determining the mean spatial orientations of bonds for each of the models we assume that the distribution of deviations of the bond directions between germanium atoms from mean orientations are specified by the Gaussian function

$$W_{\theta i}(\Delta\theta) = \frac{1}{\sqrt{2\pi}\sigma_{\theta i}} \exp\left[-\frac{\Delta\theta_i^2}{2\sigma_{\theta i}^2}\right], \tag{3}$$

where the index i numbers the germanium atom layers lying parallel to the boundary between the crystal and the amorphous layer, while $\sigma_{\theta i}$ is the standard deviation for the ith layer.

The standard deviation $\sigma_{\theta i}$ determines the extent to which the orientation of the bonds between the germanium atoms is affected by the translation symmetry of the crystal. The values of $\sigma_{\theta i}$ at $i\neq 1$ do not allow us directly to characterize the variations in the bond angle from the mean tetrahedral angle in the transition region. Only $\sigma_{\theta 1}$ can be interpreted immediately. Its value specifies the bond angle distribution of the silicon-germanium bonds constituting the crystalline-amorphous interface.

Since the orientating effect of the silicon atoms in the crystalline substrate on the positions of the germanium atoms in the transition region decreases as they grow more distant from the crystal boundary, the distribution of bond directions around the mean bond orientation becomes broader. This can be taken into account by allowing the standard deviation $\sigma_{\theta i}$ to increase from layer to layer, i.e., with increasing i. We restrict ourselves to the linear approximation for the standard deviation versus the layer number and present $\sigma_{\theta i}$ as

$$\sigma_{\theta i} = \sigma_{\theta 1} + \alpha(i-1). \tag{4}$$

The increase of $\sigma_{\theta i}$ is carried out as long as the atoms in the amorphous layer are subjected to the translation symmetry of the silicon atoms.

In determining the length of the bonds between the germanium atoms we shall assume its values to be distributed in the neighborhood of the mean value r_0 according to the Gaussian function, as is the case with bulk amorphous material,

$$W_r(r) = \frac{1}{\sqrt{2\pi}\sigma_r} \exp\left[-\frac{(r-r_0)^2}{2\sigma_r^2} \right]. \quad (5)$$

The values of r_0 and the standard deviation σ_r are believed to be constant everywhere over the amorphous region and taken to be equal to $r_0 = 0.2463$ nm and $\sigma_r = 0.0074$ nm, which are in agreement with their values for bulk amorphous germanium.[41] As a consequence, it is beyond reason to believe that the mean bond length r_0 and the standard deviation σ_r differ in the vicinity of the boundary and away from it. For the germanium atom attached to the silicon atoms the bond length r_1 is calculated as the average value between r_0 and the bond length in the silicon crystalline lattice and it equals $r_1 = 0.2408$ nm.

The introduced functions $W_{ri}(r)$ and $W_{\theta i}(\Delta\theta)$ describe the distribution of the bond lengths between the atoms in the amorphous layer and the angular distribution of those bonds relative to the mean orientations determined by the lattice built in the amorphous region. They can be used for finding the density of the mean atom distribution in the amorphous layer.

The distribution of the *j*th germanium atom in the *i*th with respect to the boundary layer is calculated based on the atom distribution in the $(i-1)$th layer. If the orientation of bonds between the germanium atoms is close to the boundary normal the atom of the *i*th layer is attached only to one atom of the $(i-1)$th layer. Let us assume that the *k*th atom of the $(i-1)$th layer is located at a point $\mathbf{r}_k$ in the amorphous part of interface. Then the function $f_{ij}(\mathbf{r})$ describing the mean density of atoms attached to this atom can be presented as

$$f_{ij}(\mathbf{r}) = W_i^{(1)}(\mathbf{r}, \mathbf{r}_k), \quad (6)$$

where $W_i^{(1)}(\mathbf{r}, \mathbf{r}_k)$ is the response function which determines the atom distribution in the *i*th layer relative to the atom positions at a point $\mathbf{r}_k$ in the $(i-1)$th layer. It is calculated using the distributions introduced as W_{ri} and $W_{\theta i}$ as

$$W_i^{(1)}(\mathbf{r}, \mathbf{r}_k) \equiv W_i^{(1)}(\mathbf{r} - \mathbf{r}_k) = C W_r(|\mathbf{r} - \mathbf{r}_k|) W_{\theta i}(\Delta\theta_i), \quad (7)$$

where $\Delta\theta_i$ is the angle between vector $(\mathbf{r} - \mathbf{r}_k)$ and the corresponding mean orientation of the bond along the [111] direction while the constant C is found with the normalization requirement taken into account,

$$\int W_i^{(1)}(\mathbf{r} - \mathbf{r}_k) d\mathbf{r} = 1. \quad (8)$$

As an approximation we suggest that response function $W_i^{(1)}(\mathbf{r}, \mathbf{r}')$ remains unchanged for every possible position $\mathbf{r}'$ of the *k*th atom in the neighborhood of the point $\mathbf{r}_k$. Then, the mean distribution of the *j*th atom in the *i*th layer attached to *k*th atom in the $(i-1)$th layer can be found as

$$f_{ij}(\mathbf{r}) = \int f_{i-1k}(\mathbf{r}') W_i^{(1)}(\mathbf{r} - \mathbf{r}') d\mathbf{r}' = f_{i-1k}(\mathbf{r}) * W_i^{(1)}(\mathbf{r}), \quad (9)$$

where $f_{i-1k}(\mathbf{r}')$ is the mean density of atoms in the vicinity of the position $\mathbf{r}_k$.

In cases where the atom of the *i*th layer is attached to three atoms of the $(i-1)$th layer the function $f_{ij}(\mathbf{r})$ is described by the expression

$$f_{ij}(\mathbf{r}) = \frac{1}{3} \sum_{k=1}^{3} \int f_{i-1k}(\mathbf{r}') W_{ijk}^{(3)}(\mathbf{r} - \mathbf{r}') d\mathbf{r}' = \frac{1}{3} \sum_{k=1}^{3} f_{i-1k}(\mathbf{r}) * W_{ijk}^{(3)}(\mathbf{r}), \quad (10)$$

where functions $W_{ijk}^{(3)}(\mathbf{r} - \mathbf{r}')$ differ from the introduced functions $W_i^{(1)}(\mathbf{r} - \mathbf{r}')$ by their indices *j* and *k* numbering three possible mean spatial bond orientations with respect to which the deviations $\Delta\theta_i$ are measured.

The three-dimensional atomic density $\rho_{3D}(\mathbf{r})$ in the amorphous part of the interface is obtained as the sum of the $f_{ij}(\mathbf{r})$ functions,

$$\rho_{3D}(\mathbf{r}) = \sum_i \sum_j f_{ij}(\mathbf{r}). \quad (11)$$

The calculations of $\rho_{3D}(\mathbf{r})$ as given above are illustrated schematically in Fig. 2 for the first two layers above the crystalline substrate. According to Eqs. (9) and (10) the density of the germanium atom distribution in the first layer parallel to the boundary is determined by functions $f_{ij}(\mathbf{r})$ at $i = 0$. They have the form

$$f_{0j}(\mathbf{r}) = \delta(\mathbf{r} - \mathbf{r}_{bj}), \quad (12)$$

where $\mathbf{r}_{bj}$'s are positions of the silicon boundary atoms assumed to be undisturbed, i.e., at this point the rigid-substrate approximation enters into the recursive scheme.

Based on the expressions presented we calculate the mean distribution of the amorphous layer atoms within the cell with the sizes (a, b, c). The values $b = 2d = 0.665$ nm and $c = 0.384$ nm correspond to the sizes of the silicon elementary cell built along the $[1\bar{1}0]$ and $[11\bar{2}]$ directions. The cell size a along the boundary normal [111] is determined by the length of the interface transition region and varied during simulating. Convolution in Eqs. (9) and (10) is easily calculated by fast Fourier transform algorithms.

After finding the mean atom distribution within the cell with the sizes (a, b, c) the two-dimensional distribution function is obtained by the expression

$$\rho(x,y) = \int_0^c \rho_{3D}(\mathbf{r}) dz. \quad (13)$$

The function $\rho(x,y)$ [Fig. 2(c)] is the basis for simulating the averaged HREM images using the APP approximation. The value $\rho(x,y)dxdy$ determines the average number of atoms in the cell (a, b, c) whose x and y coordinates are within the square $dxdy$ near the point (x,y). The features of the function $\rho(x,y)$ are varied for different models of the atom distributions in the amorphous layer of the interface and dependent on the values of the parameters $\sigma_{\theta 1}$ and α.

B. Procedure of the model parameter evaluation

To determine the optimum parameters of the *c*-Si(111)/*a*-Ge interface structure models discussed in Sec. III A and to compare the models between themselves we carried out iterative image matching for each of the models. Simulation was performed using APP approximation for the crystal thickness and 20 defocus values corresponding to the experimental through-focus series.

According to experimental investigations calculations were done for cross-section specimens imaged along [110] and illuminated by 200-keV electrons. A supercell with the sizes (a_s, b, c) was used, where $a_s = 9.406$ nm. The interface boundary was positioned at $x = 0$ close to the center of the supercell.[40] The effect of inelastic electron scattering was described by the imaginary part of the potential which was assumed to be proportional to its real part. The ratios of the imaginary part of the potential to its real part were equal to 0.05 for crystalline silicon and to 0.04 for amorphous germanium. Such a relation between the ratios yields the relationship between the mean intensities in the crystalline and amorphous parts of simulated images identical to that for experimental ones. To compare simulated and experimental images the modulation transfer function of the image recording device has been measured and taken into account as is discussed in Ref. 42. The experimental intensity distribution was scaled such that the mean intensity in the amorphous part of experimental and simulated images was equal.

For a quantitative comparison of experimental and simulated HREM images several *figures of merit* have been suggested (see, for example, Refs. 33, 34, and 43). We have found by means of computer experiments that difference measures are better suited for fitting the intensity distribution in the near interfacial image region compared to correlation measures such as the cross-correlation factor. As a difference measure we chose a sum of quadratic differences between experimental and simulated intensities, weighted by experimental intensity

$$R = \frac{1}{N}\sum_k R_k(I_{exp}^{(k)}, I_{sim}^{(k)}) = \frac{1}{N}\sum_k \sum_{ij} \frac{[(I_{exp}^{(k)})_{ij} - (I_{sim}^{(k)})_{ij}]^2}{[(I_{exp}^{(k)})_{ij}]^2} \tag{14}$$

where $I_{exp}^{(k)}$ and $I_{sim}^{(k)}$ are the intensities in one of the averaged experimental and simulated images from the defocus series consisting of $N = 20$ images, respectively, while indices i and j number points in the images.

The measure $R_k(I_{exp}^{(k)}, I_{sim}^{(k)})$ is similar to the well-known R factor used in x-ray diffraction. By using R for iterative image matching the two-dimensional distribution function can be reliably extracted from experimental data as is shown in more detail in the Appendix.

To find the optimum values of $\sigma_{\theta 1}$ and α parameters of the models proposed the figure of merit R [Eq. (14)] was minimized by the downhill simplex method.[44] As is shown by iterative image matching for the test interfaces in the Appendix this approach involving the use of the APP approximation instead of atomistic image simulations allows us to determine the parameters of the model describing the near interfacial short-range order with an accuracy of about 5%.

TABLE I. Summary of iterative image matching results. The figure of merit R is defined by Eq. (14).

Model	$\sigma_{\theta 1}$(rad)	α(rad)	R
1	0.154	0.0215	363
2	0.155	0.0207	471

C. Results of iterative image matching

First we consider interface models with one backbond of the first layer in the transition layer to the crystalline substrate. This configuration is highly favorable due to the use of the hydrophobic unreconstructed Si(111) surface as a substrate for the deposited germanium. This assumption will be justified directly from the analysis at the end of this section. The optimum values of the parameters $\sigma_{\theta 1}$, α are given in Table I for the tetragonal distorted transition region (model 1) and the undistorted transition region (model 2).

The plot of the mean two-dimensional density $\rho(x,y)$ and averaged simulated images for the respective optimum parameter values are shown for some defocus values in Figs. 3(b) and 4(b), respectively. The corresponding averaged intensity profiles obtained by Eq. (2) are presented with the experimental ones in Figs. 3(c) and 4(c).

In order to illustrate the reason for the better fit of model 1 we shall discuss the differences in the two-dimensional distribution functions of the transition layers corresponding to the two models. Figure 5 shows in addition the atomic density profiles which reveal that both models are indistinguishable in the first germanium layer and in the region beyond about 1.5 nm where $\rho(x,y)$ is nearly homogeneous, i.e., atomic positions are no longer influenced by the crystalline substrate.

The basic difference between the distribution functions in the transition layer is that spacings between the crystal and the germanium atom layers lying parallel to the boundary for the model with the ideal orientation of bonds are smaller than those for the model with tetragonal distorted bonds. As a result, the positions of maxima and minima in the averaged intensity profiles are shifted to smaller values of x for the model with the ideal orientation of bonds. Such positions of maxima and minima in the simulated intensity profiles are not in agreement with their locations in the experimental profiles [Fig. 4(c)]. The disagreement between the intensity maxima and minima positions increases as they become more distant from the boundary with the crystal. The distinctly smaller value of the measure R for the tetragonal distorted transition region compared to the undistorted case prooves the former to be the superior description of the atomic arrangements in the transition region. The fact that the two models are distinguished on the basis of the positions of intensity maxima and minima adds to the significance of this result. Unlike the true image contrasts, these positions are reliably calculated by multislice simulations with the APP approximation.[31]

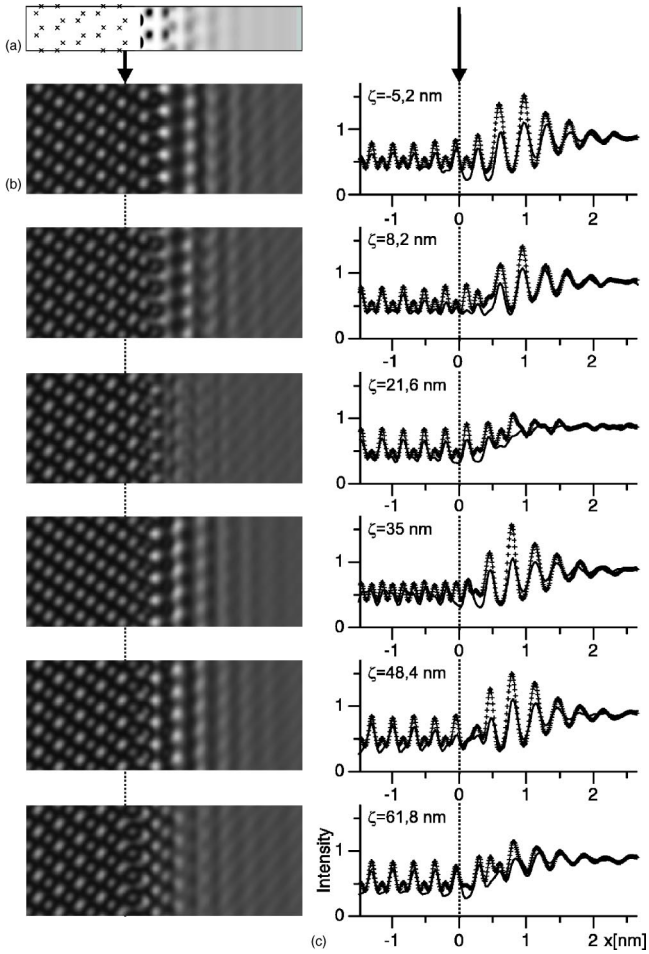

FIG. 3. Results of simulating the averaged images of the *c*-Si(111)/*a*-Ge interface using the model with tetragonal distorted bonds: (a) two-dimensional distribution of the atoms, (b) and (c) averaged images and intensity profiles, respectively. The symbols (×) in (a) show the atom positions in the crystal. In (c) the solid curves correspond to experimental intensity distributions and symbols (+) to calculated ones. The arrows indicate the position of the boundary between the crystal and the amorphous layer.

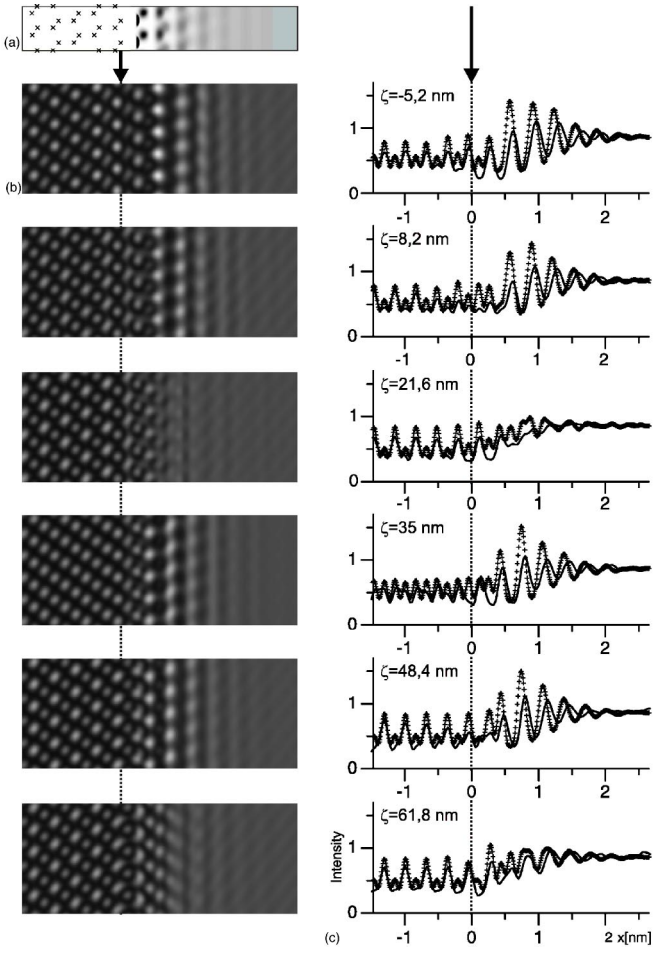

FIG. 4. Results of simulating the averaged images of the *c*-Si(111)/*a*-Ge interface using the model with the ideal orientations of bonds: (a) two-dimensional distribution of the atoms, (b) and (c) averaged images and intensity profiles, respectively. The other details are the same as in Fig. 3.

The two-dimensional distribution obtained here provides evidence for an elastic distortion of the amorphous germanium in the transition region. This distortion most likely is due to the volume misfit of crystalline silicon and amorphous germanium implying that thin amorphous films on crystalline substrates accommodate misfit similar to crystalline thin films. In this sense, thin amorphous films suffer "epitaxial" strain when deposited on crystalline substrates.[45] It should be emphasized, however, that the experimental approach used here is only sensitive in the transition region between the crystal and the amorphous bulk.

For both structure models, the value of the standard deviation for the first germanium layer is $\sigma_{\theta 1}=8.8°$. This value can be compared to the standard deviation of the bond angle distribution of bulk amorphous germanium which is equal to 9.7°,[41] and hence close to our optimum value.

Based on the $\rho(x,y)$ distribution obtained it is possible to evaluate more precisely the width w of the transition region within which the effect of the crystal translation symmetry on the atom position in the amorphous layer is preserved. Although the $\rho(x,y)$ function remains to be inhomogeneous up to $x \approx 2$ nm, its variations reduce progressively at large values of x. In order to provide a robust estimate of w, we have analyzed the effect of replacing $\rho(x,y)$ by a homogeneous distribution beyond a certain distance x_h on the quality of the iterative image matching results quantified by R [Eq. (14)]. For $x_h=1.4$ nm, $x_h=1.15$ nm, and $x_h=0.8$ nm we found that R increases by about 1% in the first case, 5% in the second case, and 40% in the last case. On this basis, the width of the transition layer is estimated as $w=1.4$ nm in the direction normal to the boundary. This value corresponds to four (111) double layers of germanium atoms consistent with the crystal structure in the [111] direction. It is considerably larger than the estimation of Tu *et al.*[17] for the *c*-Si(111)/*a*-Si interface. These authors use the variation of the energy density as a function of distance to the crystal to obtain this value. Using a bond angle criterion, da Silva *et al.*[21] obtain 1.1 nm for *c*-Si/*a*-Si with (100), (110), and (111) orientations of the crystalline silicon which is much closer to the value determined in this work.

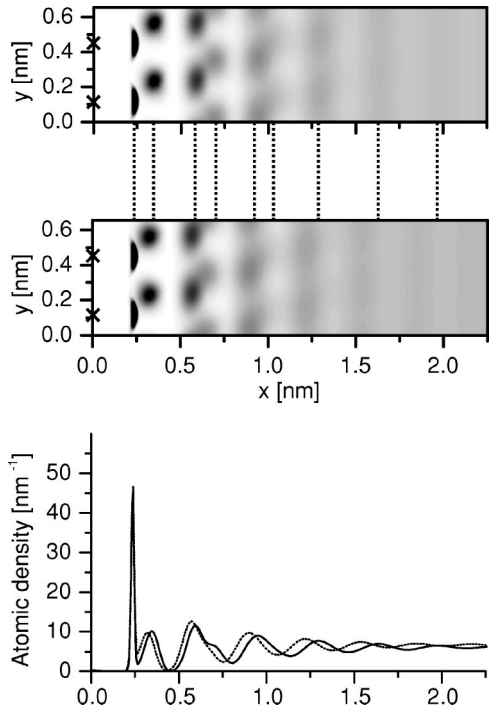

FIG. 5. The two-dimensional distribution funtions (a), (b) and atomic density profiles (c) of atoms in the amorphous part of the *c*-Si(111)/*a*-Ge interface for the model with tetragonally distorted bonds [(a) and solid curve in (c)] and the model with the ideal orientations of bonds [(b) and dashed curve in (c)]. The mean positions of the germanium atoms which form the layers lying parallel to the boundary with the crystal are compared by dashed lines.

From Fig. 5(a) it can also be seen that the mean distribution of the germanium atoms with distance from the crystal is more likely to be homogeneous along the interface than in the direction normal to the boundary. Such a regularity may be immediately noted from a qualitative analysis of the averaged experimental images [Fig. 1(e)]. This regularity testifies that structural properties and consequently other physical properties of the amorphous layer in the neighborhood of the crystal have to be different along the interface and perpendicular to it.

It is also of interest to compare atomic density profiles of the *c*-Si/*a*-Ge interface [Fig. 5(c)] with the atomic density across a liquid-solid interface.[13] In both cases layered structures arise in the disordered material near the substrate. However, for the *c*-Si/*a*-Ge interface the ordering induced by the substrate extends noticeably further into the disordered material than in the case of the solid-liquid interface.

Finally, we describe iterative image matching results for the situation where the first germanium layer has three backbonds to the silicon subtrate. The best fit yields $R=847$ which is significantly worse than the results obtained for the models with one backbond. We get $\sigma_{\theta 2}=0.166$ rad and $\alpha=0.0234$ rad. In this case parameter $\sigma_{\theta 1}$ cannot be varied in an arbitrary way. The value of $\sigma_{\theta 1}$ was estimated on the basis of the length of bond between silicon and germanium atoms r_1 and the standard deviation σ_r. It was equal to $\sigma_{\theta 1}=0.03$ rad.

The average images and the intensity profiles for this case are presented in Fig. 6. A comparatively large value of the

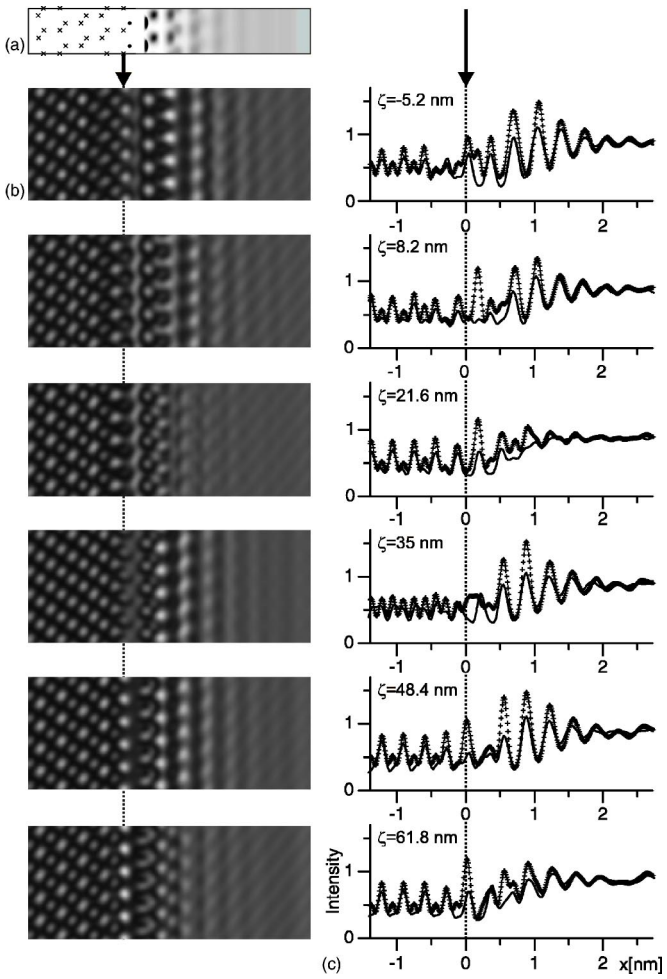

FIG. 6. Results of simulating the averaged images of the *c*-Si(111)/*a*-Ge interface using the model with tetragonal distorted bonds in the case that closest to the boundary germanium atoms are bonded with three silicon atoms: (a) two-dimensional distribution of the atoms, (b) and (c) averaged images and intensity profiles, respectively. The other details are the same as in Fig. 3.

measure R and a noticeable qualitative difference between simulated and experimental profiles in regions close to the substrate in Fig. 6(c) as compared to Fig. 3(c) are an unambiguous evidence of the fact that each of the atoms of germanium is attached to one atom of silicon. Such a conclusion is to be expected from the physical notion of the nonreconstructed hydrophobic surface of the silicon substrate where the amorphous layer of germanium was grown.

Iterative image matching does not only allow a determination of the optimum parameters of the interface structure models but also a correct estimation of the position of the boundary between the crystal and the amorphous layer. As is seen from Figs. 1, 3, 4, and 6 the boundary layer of silicon atoms is located significantly more to the left than follows from intuitive consideration based on a qualitative analysis of the averaged images with a minimal contrast in the amorphous region at $\zeta=21.6$ nm. The appearance of the crystallike contrast in the amorphous parts of the images is associated first of all with the near interfacial order of the atom positions in the amorphous layer. The effects of Fresnel dif-

fraction are also responsible for penetration of the contrast typical of the crystal inside the amorphous region of the images. The degree of penetration is dependent on the defocus and is minimal at $\zeta = 21.6$ nm.

We now discuss the causes of difference between the absolute intensity values in the experimental image and simulated ones obtained with the use of the model with tetragonal distorted bonds at the optimum parameter values. As the first cause we name the insufficiency of currently available methods of simulating HREM images which do not permit an exact calculation of intensity in the images even for a crystalline specimen because some simplifying assumptions are made in describing scattering of electrons by the specimen, imaging by the microscope optical system, and interaction with the recording device (see Ref. 46 for a review).

The second cause of difference between the theory and the experiment is some inaccuracy in determining the specimen thickness and the defocus values for images of the through-focus series, partly explained by the slightly wedge-shaped form of the specimen studied. However, as simulation shows, possible errors in the thickness and the defocus values do not produce errors in the values of the parameters $\sigma_{\theta 1}$ and α, exceeding 5%. Another factor having an effect on the accuracy of simulating the intensity in the amorphous region of HREM images, associated with shortcomings of APP approximation, will be briefly described in the Appendix and analyzed in detail in Ref. 31.

Differences between the intensity in experimental and simulated images arise also because even at the optimum values of parameters the function $\rho(x,y)$ describes the true two-dimensional distribution of atoms in the amorphous part of the interface only approximately. Inaccuracies in determining $\rho(x,y)$ are the result of the simplicity of the model used, which has only two adjustable parameters. As can be seen from Fig. 3(c) these inaccuracies are clearer pronounced within two or three germanium atom layers closest to the boundary. It is in this region of the interface that one can expect a refinement of the mean distribution function $\rho(x,y)$ when more precise methods of amorphous layer structure modeling are used.

IV. CONCLUSION

For the investigation of the transition layer between Si(111) and amorphous germanium we have analyzed HREM images of a through-focus series obtained in cross-section geometry. Averaging the images along the interface has opened the way to reveal the two-dimensional distribution function of germanium atoms which is the projection of the atomic density along the electron beam. We have made use of iterative image matching using the averaged projected potential approximation in multislice calculations. For this purpose we have developed a recursive scheme to construct the two-dimensional distribution function in terms of a small number of parameters accessible by the fitting procedure. Our analysis shows that the influence of the crystalline substrate on atomic positions in the germanium extends to about 1.4 nm from the last crystalline lattice plane of the silicon substrate. The mean orientation of bonds in the transition region provides evidence for a tetragonal distortion which is attributed to the volume misfit between crystalline silicon and amorphous germanium. From our analysis it follows that near interfacial ordering of germanium atoms together with the Fresnel diffraction effects cause the appearance of the crystal-like contrast in the amorphous part of the HREM images even for the defocus value corresponding to the minimal contrast in the image of the amorphous material. We have also found that the distribution of bond angles between the silicon substrates and the first germanium layer has a width of 8.8° compared to 9.7° for the bond angle distribution in bulk amorphous germanium. Finally, we want to mention that the two-dimensional distribution functions extracted from HREM focal series can be extracted from theoretical calculations so that their direct comparison to experiments is possible.

APPENDIX: PROCEDURE AND ACCURACY OF THE MODEL PARAMETER EVALUATION

To determine the accuracy with which the APP approximation allows us to find the parameters of the models describing the interfacial short-range order, we performed iterative image matching for test interfaces. One part of each interface with a flat boundary oriented along [111] was crystalline silicon, the second part consisted of germanium atoms randomly distributed near atomic positions corresponding to the silicon lattice; such materials will be referred to as *r*-Ge. The density of the germanium atoms' distribution was specified by the Gaussian function

$$f_{ij}(x,y,z) = \frac{1}{2\pi\sigma_{xi}\sigma_{yi}} \exp\left(-\frac{(x-x_{ij})^2}{2\sigma_{xi}^2}\right)\exp\left(-\frac{(y-y_{ij})^2}{2\sigma_{yi}^2}\right), \tag{A1}$$

$x_{ij} = x'_{ij} + \beta_r \sigma_{xi}$, x'_{ij} and y_{ij} are the coordinates of the jth position of the silicon lattice in the ith layer. The atom coordinates along the z axis matched with crystal positions. The standard deviation were calculated as

$$\sigma_{xi} = \sigma_{yi} = \sigma_1 + \alpha_r(i-1). \tag{A2}$$

The dependence of coordinate x_{ij} on σ_{xi} and hence on the layer number made it possible to vary the average spacing between the layers of germanium atoms lying parallel to the boundary. Introduction of such a dependence for the test interface is caused by the fact that variations of the average interlayer spacing as they become more distant from the boundary are typical for the models of crystalline-amorphous interfaces considered.

The averaged HREM images of test interfaces were simulated using conventional atomistic simulations or the APP approximation. The specimen orientation and the microscope parameters were the same as in Sec. III. The ratios of the imaginary part of the potential to its real part were equal to 0.05 for both sorts of atoms.

For atomistic simulations a supercell with the sizes $(a, 14b, c)$ was used, where $a = 9.406$ nm, $b = 0.665$ nm, $c = 0.384$ nm. The interface boundary was positioned in the middle of the supercell $(x = a/2)$, while the atoms of germa-

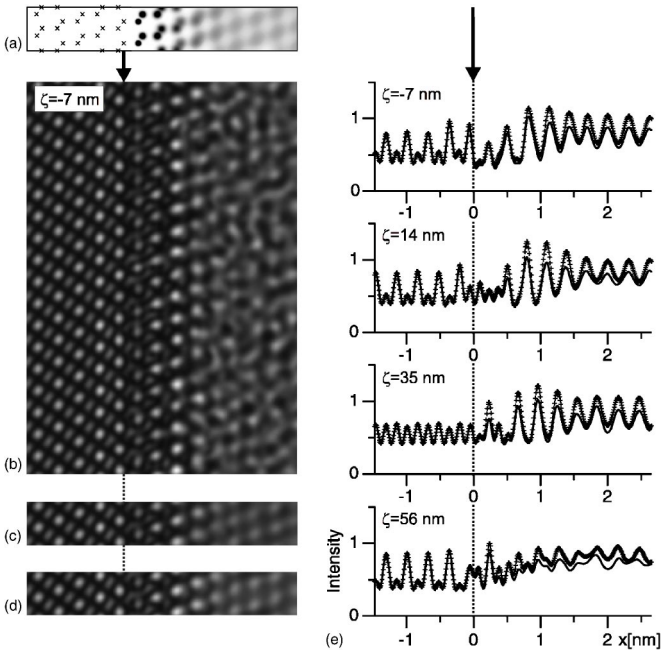

FIG. 7. Simulation of the HREM images for the test *c*-Si/*r*-Ge interface. (a) shows the two- dimensional distribution of the atoms where the atom positions in the crystal are illustrated by the (x) symbols, (b) section of the simulated HREM image, (c) result of its averaging, (d) averaged image calculated using APP approximation, (e) averaged intensity profiles for the given defocus values. Solid curves correspond to atomistic calculations and (+) symbols to simulations using the APP approximation.

nium with $x > a/2$ were distributed according to Eq. (A1). The images were simulated for 20 defocus values in the $\zeta = -35\text{-nm} - \zeta = 98\text{-nm}$ range with an increment of $\Delta\zeta = 7$ nm. The specimen thickness was 13.8 nm. Figure 7 shows simulated images of the *c*-Si/*r*-Ge interfacial region (a) and associated averaged image (b) for $\sigma_{r1} = 0.02$ nm, $\alpha_r = 0.008$ nm, and $\beta_r = 1.5$. The corresponding average two-dimensional atom distribution calculated within the cell (a_s, b, c) and projected onto the *xy* plane according to Eq. (13) is shown in Fig. 7(a). Such a distribution of germanium atoms for test simulation was chosen because it is qualitatively similar to the two-dimensional atom distribution $\rho(x,y)$ of the real *c*-Si(111)/*a*-Ge interface [see Sec. III C, Fig. 3(a)].

For APP approximation averaged images were simulated using mean two-dimensional functions of the germanium atom distribution obtained by Eqs. (11), (13), (A1), and (A2). The sizes of the supercells *a* and *c*, the boundary position, and the microscope parameter were the same as in the first case. The supercell size along the *y* axis was equal to *b*. The values of parameters σ_1 and α_r were determined by iterative matching the averaged images calculated using APP approximation with those obtained by an atomistic simulation. Differences between the images obtained with the two methods were characterized to the figure of merit equivalent to Eq. (14) whose value was calculated and minimized as described in Sec. III B.

TABLE II. Summary of iterative image matching results for the test interface described by input parameters $(\sigma_1)_{at}$ and α_{at}; $(\sigma_1)_{APP}$ and α_{APP} denote the results of iterative image matching using the APP approximation.

$(\sigma_1)_{at}$(nm)	α_{at}(nm)	$(\sigma_1)_{APP}$(nm)	α_{APP}(nm)
0.020	0.008	0.0207	0.00764
0.026	0.007	0.0256	0.00690

Matching the averaged images obtained using APP approximation with the atomistic calculated images was performed for several sets of the σ_{r1}, α_r, and β_r parameter values. The results obtained for two of them are summarized in Table II showing that the input parameters are retrieved with a high accuracy by the image matching procedure using the APP approximation.

The parameter β_r was not varied; its value was 2 in the first case and 1.5 in the second case.

It follows from the data presented that if two-dimensional distribution functions of the test interface is qualitatively similar to the average distribution functions of the amorphous layer atoms in the vicinity of the interface then the error in determining σ_{r1} and α_r parameters by simulating the averaged HREM images using APP approximation is less than 5%.

The averaged image calculated with the APP approximation for the first set of parameters and one of the defocus values is shown in Fig. 7(d). As is clear from Figs. 7(c) and 7(d) the intensity distributions in the images obtained by two simulation methods are close to each other. From Fig. 7(e) it can be seen that for all defocus values the character of the intensity distribution is the same and the positions of maxima and minima coincide. Between the absolute intensity values calculated by atomistic simulations and those obtained with the use of APP approximation there are differences which become more pronounced in the vicinity of the intensity maxima. Those differences are mainly due to the inaccuracy of APP approximation which does not allow one to take an exact account of a part of the contributions into the intensity, arising from the scattering of fast electrons by the specimen. However, since within the APP approximation the dominating contributions into the averaged intensity are correctly described, application of APP approximation makes it possible to determine the σ_{r1} and α_r parameters of the interface structure with a good accuracy.

*Permanent address: Moscow Institute of Electronic Technology, 103498 Moscow, Russia.
†Present address: Infineon Technologies AG, Wernerwerkstr. 2, D-93049 Regensburg, Germany.
‡Electronic address: seibt@ph4.physik.uni-goettingen.de

[1] F. Priolo and E. Rimini, Mater. Sci. Rep. **5**, 319 (1990).
[2] A.G. Cullis, N.G. Chew, H.C. Webber, and D.J. Smith, J. Cryst. Growth **68**, 624 (1984).
[3] D.J. Eaglesham, J. Appl. Phys. **77**, 3597 (1995).
[4] R. Chau, J. Kavalieros, B. Roberds, R. Schenker, D. Lionberger, D. Barlage, B. Doyle, R. Arghavani, A. Murthy, and G. Dewey, Tech. Dig. - Int. Electron Devices Meet. **2000**, 45 (2000).
[5] J.S. Moodera, L.R. Kinder, T.M. Wong, and R. Meservey, Phys. Rev. Lett. **74**, 3273 (1995).
[6] M. Münzenberg and J.S. Moodera, Phys. Rev. B **70**, 060402(R) (2004).
[7] P. Gaskell, in *Glasses and Amorphous Materials*, edited by J. Zarzycki, Vol. 9 of Materials Science and Technology, edited by R.W. Cahn, P. Haasen, and E.J. Kramer (VCH, Weinheim, 1991).
[8] A. Filiponi, F. Evangilisti, M. Benfatto, S. Mobilo, and C.R. Natoli, Phys. Rev. B **40**, 9636 (1989).
[9] M.M.J. Treacy and J.M. Gibson, Acta Crystallogr., Sect. A: Found. Crystallogr. **52**, 212 (1996).
[10] J.M. Gibson and M.M.J. Treacy, Phys. Rev. Lett. **78**, 1074 (1997).
[11] H. Löwen and T. Beier, Phys. Rev. B **41**, 4435 (1990).
[12] F. Spaepen, Solid State Phys. **47**, 1 (1994).
[13] W. Huisman, J.F. Peters, M.J. Zwanenburg, S.A. de Vries, T.E. Derry, D. Abernathy, and J.F. van der Veen, Nature (London) **390**, 379 (1997).
[14] P. Geysermans, D. Gorse, and V. Pontikis, J. Chem. Phys. **113**, 6382 (2000).
[15] F. Spaepen, Acta Metall. **26**, 1167 (1978).
[16] N. Bernstein, M.J. Aziz, and E. Kaxiras, Phys. Rev. B **58**, 4579 (1998).
[17] Y. Tu, J. Tersoff, G. Grinstein, and D. Vanderbuilt, Phys. Rev. Lett. **81**, 4899 (1998).
[18] Y. Tu and J. Tersoff, Phys. Rev. Lett. **84**, 4393 (2000).
[19] R. Buczko, S.J. Pennycook, and S.T. Pnatelides, Phys. Rev. Lett. **84**, 943 (2000).
[20] M. Peressi, L. Colombo, and S. de Gironcoli, Phys. Rev. B **64**, 193303 (2001).
[21] C.R.S. da Silva and A. Fazzio, Phys. Rev. B **64**, 075301 (2001).
[22] N. Bernstein, M.J. Aziz, and E. Kaxiras, Phys. Rev. B **61**, 6696 (2000).
[23] D.M. Stock, B. Weber, and K. Gärtner, Phys. Rev. B **61**, 8150 (2000).
[24] Y. Tu and J. Tersoff, Phys. Rev. Lett. **89**, 086102 (2002).
[25] S.M. Goodnick, D.K. Ferry, C.W. Wilmsen, Z. Liliental, D. Fathy, and O.L. Krivanek, Phys. Rev. B **32**, 8171 (1985).
[26] I. Ohdomari, T. Mihara, and K. Kai, J. Appl. Phys. **59**, 2798 (1986).
[27] A. Ourmazd, D.W. Taylor, J.A. Rentschler, and J. Bevk, Phys. Rev. Lett. **59**, 213 (1987).
[28] H. Akatsu, Y. Sumi, and I. Ohdomari, Phys. Rev. B **44**, 1616 (1991).
[29] N. Ikarashi, K. Watanabe, and Y. Miyamoto, Phys. Rev. B **62**, 15 989 (2000).
[30] M. Howe, Philos. Mag. A **74**, 761 (1996).
[31] N.I. Borgardt, B. Plikat, M. Seibt, and W. Schröter, Ultramicroscopy **90**, 241 (2002).
[32] P. Goodman and A.F. Moodie, Acta Crystallogr., Sect. A: Cryst. Phys., Diffr., Theor. Gen. Crystallogr. **30**, 280 (1974).
[33] G. Möbus, R. Schweinfest, T. Gemming, T. Wagner, and M. Rühle, J. Microsc. **190**, Pts. 1/2, 109 (1998).
[34] G. Möbus, in *High-Resolution Imaging and Spectrometry of Materials*, edited by F. Ernst and M. Rühle, Springer Series in Materials Science No. 50 (Springer, Berlin, 2003), p. 69.
[35] W. Coene, G. Janssen, M. Op de Beeck, and D. van Dyck, Phys. Rev. Lett. **69**, 3743 (1992).
[36] M. Suhren, D. Gräf, R. Schmolke, H. Piontek, and P. Wagner, Inst. Phys. Conf. Ser. **149**, 301 (1996).
[37] U. Neuwald, H.E. Hessel, A. Feltz, U. Memmert, and R.J. Behm, Appl. Phys. Lett. **60**, 1307 (1992).
[38] Please note that throughout this work the objective lens defocus has positive values in the case of underfocus. Hence the value of $\zeta = 21.6$ nm corresponds to the *minimum-contrast* condition.
[39] F. Wooten, K. Winer, and D. Weaire, Phys. Rev. Lett. **54**, 1392 (1985); F. Wooten and D. Weaire, Solid State Phys. **40**, 1 (1987).
[40] As microscope parameters we used a spherical aberration coefficient of 0.48 mm, a convergence semiangle of 0.1 mrad, an aperture diameter of 24 mrad and a spread of focus of 2.4 nm.
[41] G. Etherington, A.C. Wright, J.T. Wenzel, J.C. Dore, J.H. Clarke, and R.N. Sinclair, J. Non-Cryst. Solids **48**, 265 (1982).
[42] J.M. Zuo, Ultramicroscopy **66**, 21 (1996).
[43] R. Hillebrand and H. Hofmeister, Phys. Status Solidi A **150**, 65 (1995).
[44] W.H. Press, S.A. Teukolsky, W.T. Vettering, and B.P. Flannery, *Numerical Recipes* (Cambridge University Press, Cambridge, England, 1992).
[45] J.A. Floro, P.G. Kotula, S.C. Seel, and D.J. Srolovitz, Phys. Rev. Lett. **91**, 096101 (2003).
[46] C.B. Boothroyd, J. Microsc. **190**, Pts. 1/2, 99 (1998).